Coherence, collective rhythm, and phase difference distribution in populations of stochastic genetic oscillators with cellular communication

Zhanjiang Yuan,[1] Jiajun Zhang,[1] and Tianshou Zhou[1,2,*]
[1]*School of Mathematics and Computational Science, Sun Yat-Sen University, Guangzhou 510275, China*
[2]*State Key Laboratory of Biocontrol and Guangzhou Center for Bioinformatics, School of Life Science, Sun Yat-Sen University, Guangzhou 510275, China*
(Received 3 March 2008; revised manuscript received 25 April 2008; published 2 September 2008)

An ensemble of stochastic genetic relaxation oscillators via phase-attractive or repulsive cell-to-cell communication are investigated. In the phase-attractive coupling case, it is found that cellular communication can enhance self-induced stochastic resonance as well as collective rhythms, and that different intensities of noise resulting from the fluctuation of intrinsic chemical reactions or the extrinsic environment can induce stochastic limit cycles with different amplitudes for a large cell density. In contrast, in the phase-repulsive coupling case, the distribution of phase differences among the stochastic oscillators can display such characteristic as unimodality, bimodality or polymodality, depending on both noise intensity and cell number, but the modality of phase difference distribution almost keeps invariant for an arbitrary noise intensity as the cell number is beyond a threshold.

DOI: 10.1103/PhysRevE.78.031901 PACS number(s): 87.16.Yc, 05.40.−a, 05.45.Xt

I. INTRODUCTION

Gene regulation processes in *in vivo* cells are performed by complex networks which include interactions at the level of transcriptional regulation as well as post-transcriptional regulation by protein-protein interactions [1,2]. Periodic changes in protein abundances are at the heart of important cellular processes, which can play essential roles in keeping time in organisms, encoding information for cell signaling, coordinating diverse cellular processes, etc. [3,4]. Relevant examples include self-sustained oscillations in circadian clocks, enzyme syntheses, and cell cycles [5]. On the other hand, synthetic gene regulatory networks have the potential to enhance our understanding of important cellular processes and receive increasing attention mainly due to their advantages, e.g., they can be taken as substitutes to natural gene networks for detailed study. Several oscillator architectures have been developed and implemented in experiments [6–8]. Of these synthetic genetic oscillators, an interesting yet typical example is genetic relaxation oscillator that can be constructed by embedding positive and negative feedback loops into a gene network. Such a genetic oscillator displays relaxation oscillation, and is a prevalent molecular oscillator motif in many circadian rhythms and cell cycles across many organisms [9,10].

From dynamical viewpoints, self-sustained oscillating behaviors in nonlinear systems can be offered by limit cycles. Even in the absence of limit cycle, however, internal rhythms can also be generated in nonlinear systems due to the effect of noise. Such a phenomenon is so-called noise-induced coherent motion which has become an active topic mostly driven by its enormous relevance in numerous applications in such fields as engineering, physics, biology, and medicine [11–14]. In this paper we call such a noise-induced oscillator as stochastic oscillator. Its basic dynamical characteristic is that the corresponding deterministic system does not oscillate and is actually near but before a Hopf bifurcation point. Owing to the constructive effect of noise, however, the original potential limit cycle is excited. It has been verified that noise-induced oscillations can be deterministic in suitable limits [15–19]. Such stochastic genetic oscillators can exist in many biological systems. For example, the noise-excited competent state in *Bacillus subtilis* corresponds to the slow relaxation of an excitable system [20–22]. In addition, some genetic systems in a deterministic setting never flip from low states to high states, but stochastic fluctuations can flip this switch and allow the systems to oscillate [3,23,24].

Given that cells are frequently subject to chemical signals from their neighboring cells, it is worth studying the effect of such chemical communication on the dynamics of populations of genetic oscillators, especially in the case of stochastic genetic oscillators. It has been shown that an ensemble of repressilators coupled to a quorum-sensing apparatus behave like a macroscopic genetic clock [25], displaying a robust collective rhythm in a manner that the coupling reduces the noisiness of the system. A more detailed work is that cell-to-cell communication can synchronize genetic relaxation oscillators, where the dominant mechanism of the synchronization process is "fast threshold modulation" [26]. Even in the fluctuated cellular environment, the joint effect of chemical signals and noises not only can coordinate cellular behaviors in a synchronous manner but also can lift the dynamics of individual cells from a steady state to a stochastic limit cycle [27]. We note that collective behaviors in these interacting biological systems are achieved by the so-called phase-attractive cell-to-cell communication module, or simply attractive coupling. However, coupling can be devised in different ways in synthetic biological systems. Recently, a phase-repulsive cellular communication module has been proposed [28]. In contrast to attractive coupling, repulsive coupling has different effects on cellular population behaviors, e.g., clustering and multistability [28]. Actually, repulsive (or inhibitory) coupling is very common in a biological

*mcszhtsh@mail.sysu.edu.cn

system. In Ref. [29], it was shown that sparse long-range repulsive coupling as well as local attractive coupling can produce the stable uniform phase distributions in an array of identical phase oscillators. With repulsive coupling, moreover, identical phase oscillators coupled in a two-dimensional array manner show the phase shift π [30], etc.

A naturally arising question is how phase-attractive and repulsive cell-to-cell communications affect coherence and collective rhythms across an ensemble of stochastic genetic oscillators. How does one describe collective behaviors? In this paper, we take a stochastic relaxation-type genetic oscillator capable of generating reliable rhythms in the presence of fast molecular noise as the core module to address these questions. We focus on the effects of noise, cell density, and cellular communication on coherence and collective behaviors in a population of the stochastic genetic oscillators. We show that information exchange between cells via the attractive coupling can enhance the coherence of individual cells and induce robust collective behaviors. On the other hand, in the case of repulsive coupling, the distribution function of phase difference among stochastic oscillators can display unimodality, bimodality or polymodality, depending on the noise intensity and the cell number.

II. STOCHASTIC GENETIC OSCILLATOR AND ITS BASIC DYNAMICS

Rhythm generation is a long-term topic in biological and cognitive sciences [31,32]. Understanding the mechanism of rhythm generation is a basic yet significant task. Except for the fact that self-sustained oscillating behaviors in nonlinear systems are mostly offered by limit cycles, internal rhythms can be also generated in nonlinear systems even in the absence of a limit cycle, mainly due to the effect of noise. A system with such a noise-induced coherent motion will be called a stochastic oscillator.

In order to provide some insights into noise-induced rhythms and after-displayed collective behaviors in populations of stochastic genetic oscillators, in this section we consider a synthetic genetic relaxation oscillator motif proposed by Hasty *et al.* [25,33]. In this motif, two genes produce activator (x) and repressor (y), respectively, under the control of the same promoter, and the repressor antagonizes the activator action, e.g., it acts as a protease by increasing the activator degradation linearly. The synthetic network is shown in Fig. 1(a). The time evolution of concentrations of the proteins can be determined by the following deterministic equations:

$$\frac{dx}{dt} = \alpha_1 \frac{1+\rho x^n}{1+x^n} - \beta_1 x - \gamma x y, \tag{1}$$

$$\frac{dy}{dt} = \alpha_2 \frac{1+\rho x^n}{1+x^n} - \beta_2 y, \tag{2}$$

where variables x and y represent activator and repressor, respectively. Parameters α_i $(i=1,2)$ are the dimensionless transcription rates in the absence of activator, β_i $(i=1,2)$ are the degradation rates, γ is the repressor strength, $\rho>0$ represents the increase of a protein production due to the binding of the activator to the promoter, and n is the Hill coefficient. From dynamical viewpoints, the above system possesses rich dynamics, which results mainly from the structure composed of fast positive feedback and slow negative feedback. Figure 1(b) shows a bifurcation diagram of the system (1) and (2) with respect to the parameter γ. Clearly, the system has only a stable fixed point corresponding to the quiescent state when $\gamma<3.81$ or $\gamma>24.46$, whereas there exists a globally stable limit cycle when γ falls into (3.81 24.46). Also, Fig. 1(c) displays a phase diagram in the phase plane (x,y) in an oscillation setting.

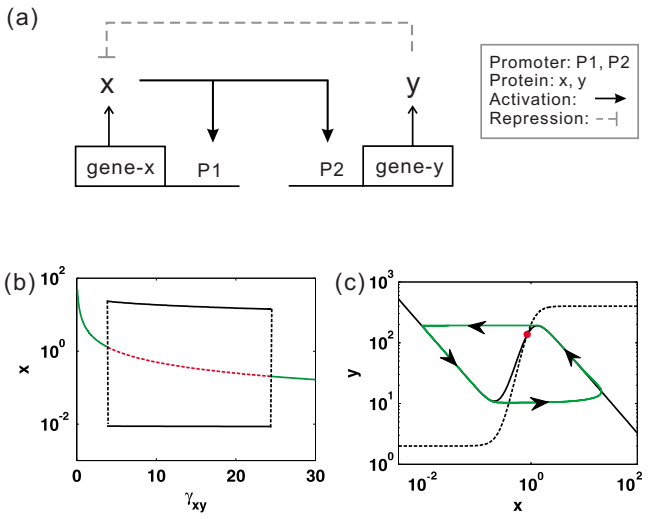

FIG. 1. (Color online) A genetic relaxation system and its basic dynamics. (a) The scheme of gene regulatory network; (b) the bifurcation diagram, where the solid lines represent the stable fixed point (green) or limit cycle (black) in which the maximal-minimal amplitudes of oscillation are plotted. Bifurcation points are $\gamma^l=3.81$ (left-hand side), $\gamma^r=24.46$ (right-hand side); (c) nullclines and limit cycle trajectories (green), where black solid and dotted lines represent x and y nullclines, respectively, and the red dot is the unique unstable fixed point. Parameter values are $\alpha_1=10$, $\alpha_2=1$, $\beta_1=0.5$, $\beta_2=0.5$, $\rho=200$, $n=4$. $\gamma=6$ in (c).

Based on the detailed-above dynamical result, we next focus on noise-induced coherent motions, i.e., stochastic rhythms in a noisy environment, where the deterministic system cannot oscillate, e.g., for the parameter $\gamma=3$, the system is at a stable steady state [see Fig. 1(b)]. Note that noise in the form of random fluctuations arises in different ways in genetic systems, e.g., internal noise results from the relatively small number of reactant molecules, and external noise originates in the random variation of one or more of the externally set control parameters [34–36]. If the noise source is small, its effect can be often incorporated *post hoc* into the rate equations [37,38]. Here, for model (1) and (2) we introduce a stochastic fluctuation to the parameter γ, i.e., $\gamma \to \gamma + \xi(t)$ in which $\langle \xi(t) \rangle = 0$, $\langle \xi(t)\xi(t') \rangle = D\delta(t-t')$ with D representing the intensity of the noise $\xi(t)$. In addition, we also introduce an environmental fluctuation in the model, i.e., the addition of $\xi(t)$ to the equation of the variable x (data not shown). In both cases, importantly, the stochastic oscillators are generated through the so-called self-induced stochastic

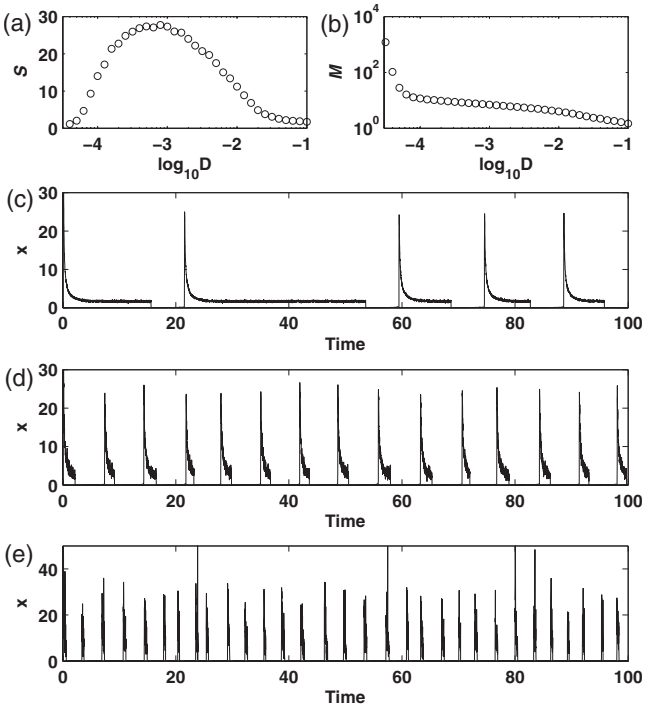

FIG. 2. Dynamics of the stochastic genetic oscillator. (a) The signal-to-noise ratio S as a function of noise intensity D; (b) the mean firing period M as a function of D; (c), (d), and (e) the time evolution of the component x, where (c) corresponds to $D=10^{-4.2}$, (d) to $D=10^{-3.0}$, and (e) to $D=10^{-1.8}$.

resonance (SISR) mechanism since the noises perturb the fast variable (x) [17–19]. All involved stochastic equations throughout this paper are numerically solved using the Heun algorithm with step size $\Delta=10^{-3}$ [39].

To measure the temporal coherence of noise-induced oscillations, we introduced an index, denoted by S and defined as [13]

$$S=\frac{\langle T_k\rangle_t}{\sqrt{\mathrm{var}(T_k)}} \tag{3}$$

$T_k=\tau_{k+1}-\tau_k$ (here τ_k is the time until the presence of the kth firing of the noise-induced oscillator) stands for the distribution of pulse duration, and $\langle\cdots\rangle_t$ denotes average over time. Such an index describes a ratio between the average of interspike interval and its standard deviation, and is actually a kind of signal-to-noise ratio in the sense of periodic signals repetitive at a fixed interval. The bigger the index S, the higher the coherence degree of output signals. In Fig. 2(a), we show the S as a function of the noise intensity D, where there exists an optimal noise such that S has the maximum. In addition, we also investigate the influence of noise on mean firing period which is defined as $M=\langle T_k\rangle_t$. The results are shown in Fig. 2(b). Apparently, M decreases with the increase of D. Therefore, the noise intensity can serve as a controllable parameter for the mean firing period. Three typical numerical realizations of the noise-induced dynamics under different noise intensities are demonstrated in Figs. 2(c)–2(e), respectively. When the noise is rather small or large, the system does not display regular coherent motion,

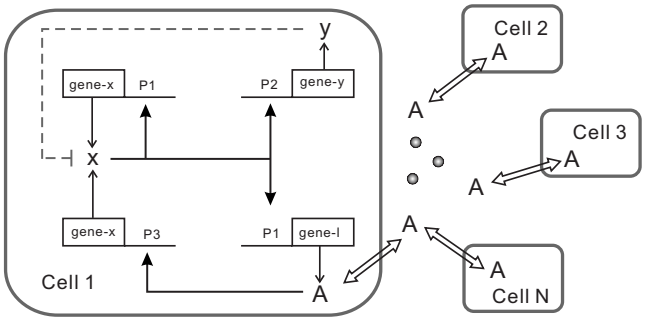

FIG. 3. Scheme of the stochastic genetic oscillator coupled to a quorum-sensing mechanism apparatus via attractive phase. x and y denote the proteins, and $P1$, $P2$, and $P3$ the promoters. The symbol A refers to the signaling molecules. The hollow bidirectional arrow denotes the diffusion of signaling molecules across the cellular membrane.

as shown in Figs. 2(c) and 2(e), respectively. However, in Fig. 2(d) the moderate noise intensity can induce pronouncedly regular stochastic oscillation, which can almost compare favorably with deterministic periodic motion shown in Fig. 1(c).

III. ATTRACTIVE COUPLING: COHERENCE, SYNCHRONIZATION AND NOISE-INDUCED STOCHASTIC LIMIT CYCLES WITH DIFFERENT AMPLITUDES

Cells may exchange chemical signals via some small molecules in various forms and receive fluctuated stimuli simultaneously from their neighboring units. Among types of cellular communication, the quorum sensing is one of prevalent and programable mechanisms in cell populations. Here, we adopt this mechanism to communicate in an ensemble of stochastic genetic oscillators. The similar mechanisms have been also adopted in Refs. [25–27,40,41], but therein each genetic oscillator is a self-sustained one. The scheme of the stochastic genetic network coupled to a quorum-sensing mechanism is shown in Fig. 3, and the corresponding dynamical equations are given by

$$\frac{dx_i}{dt}=\alpha_1\frac{1+\rho x_i^n}{1+x_i^n}-\beta_1 x_i-[\gamma+\xi_i(t)]x_i y_i+\mu\frac{1+\rho_1 A_i^2}{1+A_i^2}, \tag{4}$$

$$\frac{dy_i}{dt}=\alpha_2\frac{1+\rho x_i^n}{1+x_i^n}-\beta_2 y_i, \tag{5}$$

$$\frac{dl_i}{dt}=\alpha_3\frac{1+\rho x_i^n}{1+x_i^n}-\beta_3 l_i, \tag{6}$$

$$\frac{dA_i}{dt}=\alpha_4 l_i-\beta_4 A_i+\eta_{\mathrm{int}}\left(\frac{Q}{N}\sum_{j=1}^{N}A_j-A_i\right), \tag{7}$$

where the meaning of variables x_i and y_i and some parameters is the same as that in Eqs. (1) and (2). Variables l_i, and A_i are the components of communication apparatus in the

quorum-sensing mechanism. Parameters α_3, α_4, and μ are the dimensionless transcription rates, β_3 and β_4 are the degradation rates, $\rho_1 > 0$ represents the increase of the protein production due to the binding of the signal molecule to the promoter, η_{int} is the diffusion rate of A_i across the cell membrane, and $\xi_i(t)$ is an independent Gaussian noise satisfying $\langle \xi_i(t) \rangle = 0$. $\langle \xi_i(t)\xi_j(t') \rangle = D\delta_{ij}\delta(t-t')$ $(i,j=1,2,\ldots,N)$ with D being the noise intensity. According to Ref. [25], we know the parameter $Q = \frac{\omega N/V_{\text{ext}}}{k_e+\omega N/V_{\text{ext}}}$ with $\omega N/V_{\text{ext}} = k_{\text{diff}}$ being the diffusion rate. Therefore, Q depends on N in a nonlinear way but we can take Q as a controller parameter to represent the cell density. Throughout this section, we fix the parameters as follows: $\alpha_1 = 10$, $\alpha_2 = 1$, $\alpha_3 = 50$, $\alpha_4 = 0.4$, $\beta_1 = 0.5$, $\beta_2 = 0.5$, $\beta_3 = 25$, $\beta_4 = 0.2$, $\rho = 200$, $\rho_1 = 10$, $\gamma = 3.8$, $\mu = 10$, $n = 4$, $\eta_{\text{int}} = 120$.

To understand the dynamics of the multicelluar system with the phase-attractive communication, we rewrite Eq. (7) as

$$\frac{dA_i}{dt} = \alpha_4 l_i - \beta_4 A_i - \eta_{\text{int}}(1-Q)A_i + \frac{\eta_{\text{int}} Q}{N}\sum_{j=1}^{N}(A_j - A_i). \tag{8}$$

Note that the synchronized solution of the entire system (4)–(7) does not consist of the solutions of the uncoupled individual cell systems (1) and (2), but those of Eqs. (4)–(7) plus the following equation:

$$\frac{dA_i}{dt} = \alpha_4 l_i - \beta_4 A_i - \eta_{\text{int}}(1-Q)A_i. \tag{9}$$

For convenience, we call the system consisting of Eqs. (4)–(6) and (9) as auxiliary system. To that end, we display a bifurcation diagram of the auxiliary system, referring to Fig. 4(a). Theoretical and simulation analysis shows that the auxiliary model belongs to type II classified for neuronal models in Refs. [42–44]. Specifically, the system has a stable single equilibrium point when it does not oscillate, and the equilibrium point loses stability and generates a subcritical Hopf bifurcation as the parameter γ changes. However, the bifurcation diagram near the bifurcation point is not easily and clearly shown because the subcritical Hopf bifurcation point is very close to the bifurcation point of the saddle-node type, leading to two vertical lines. As seen from Fig. 4(a), the cell density Q can greatly influence the intrinsic dynamics by decreasing the oscillation amplitude significantly. Figure 4(b) displays the corresponding phase diagram of limit cycles in the phase plane (x,y) for two different cell densities, where there is an obvious difference between the two limit cycles. Besides, the asymmetry of coupling has some other effects on the intrinsic dynamics, e.g., with the increase of value of Q, the value of γ evaluated at the left bifurcation point (excitation threshold) shows some increase, as shown in Fig. 4(c). In other words, the increase of Q can lift the excitation threshold. For a fixed γ near but after the corresponding bifurcation point, the maximal activation of the component x shows first a small change as Q varies, and then a rapid decrease when Q approaches to 1, as clearly seen from Fig. 4(d).

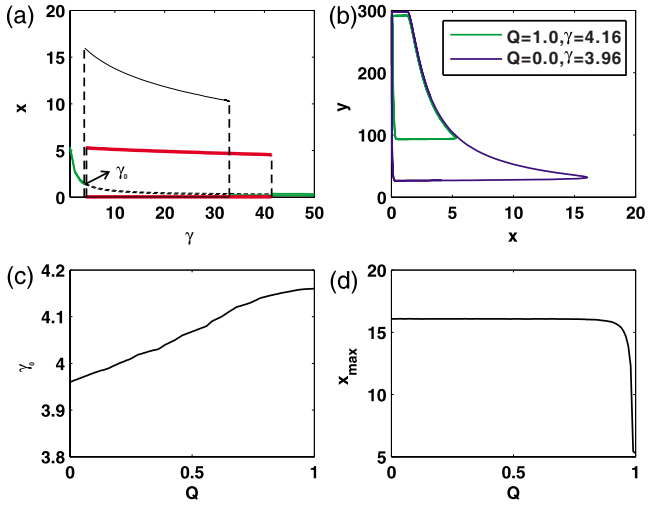

FIG. 4. (Color online) (a) The bifurcation diagram for the auxiliary system, where the solid lines represent the stable fixed point (green) or limit cycle, and the dashed line in between two solid curves represents the unstable fixed point. In the case of limit cycle, the maximal-minimal amplitudes of oscillation are plotted, where $Q=0.0$ (thin black line), $Q=1.0$ (thick red line) with γ being in the interval of oscillation, γ_0 represents a subcritical Hopf bifurcation point; (b) two typical limit cycle trajectories, where the blue corresponds to $Q=0.0$ and $\gamma=3.96$ whereas the green corresponds to $Q=1.0$ and $\gamma=4.16$; (c) the dependence of the bifurcation point γ_0 on Q; (d) the maximal activation of the component x vs Q, where the γ takes the values that are determined in (c).

Next, we investigate the effects of multiplicative noise and additive noise (assume that additive noise is added to the equation of the fast variable x) on the auxiliary system. Figures 5(a) and 5(b) show S as a function of noise intensity D and cell density Q in the cases of multiplicative and additive noises, respectively. One can see from these two figures that S has the maximum with respect to the noise intensity for a fixed Q, which is attributed to the SISR mechanism. However, the phase portraits in the cases of these two types of noises display obvious differences, as shown in Figs. 5(c) and 5(d). For weak noise intensities in both situations, the stochastic limit cycles are essentially the precursors of the deterministic limit cycle generated by Hopf bifurcation. With the increase of the noise intensity, the difference of the phase portraits gradually appears. In the case of multiplicative noise, the maximal activation of the protein x with stochastic oscillation shows small changes but the maximal activation of the protein y is greatly influenced by the noise, displaying the monotonic decrease with the increase of noise intensity, referring to Fig. 5(c). On the other hand, in the case of additive noise, the maximal activation of the protein x shows significant changes, sliding down remarkably with the increase of noise intensity, but the maximal activation of the protein y shows small changes. These numerical results further indicate the pronounced characteristic of the SISR effect.

Based on the SISR idea of Lee DeVille, *et al.* [17,18] and Freidlin [45], here we give some explanations in order to better understand the above jump mechanism. Note that the dynamical equation describing the fast variable can be written as

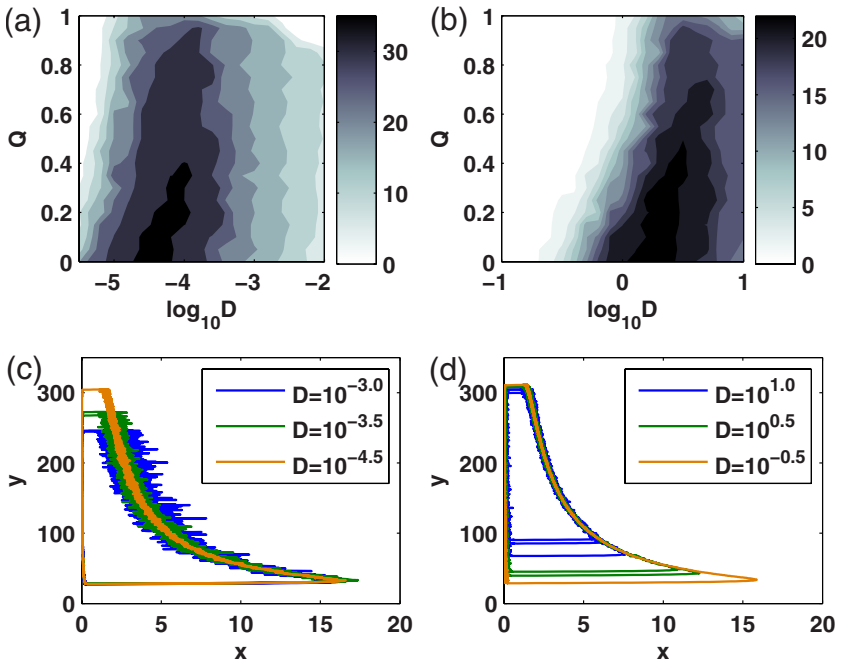

FIG. 5. (Color online) The signal-to-noise ratio S as a function of noise intensity D and cell density Q when the auxiliary system is subjected to multiplicative noise (a); additive noise (b). Typical stochastic oscillatory behaviors induced by weak, moderate, and strong multiplicative noises (c); additive noises (d), respectively. In the cases of (c) and (d), $Q=0.8$.

$$\frac{dx}{dt} = \alpha_1 \frac{1+\rho x^n}{1+x^n} - \beta_1 x - \gamma xy + \mu \frac{1+\rho_1 A^2}{1+A^2} + \sigma(x,y)\xi(t)$$

$$\triangleq f(x,y,A) + \sigma(x,y)\xi(t), \tag{10}$$

where $\sigma(x,y)=$const. for additive noise and $\sigma(x,y)=xy$ for multiplicative noise. Furthermore, Eq. (10) can be rewritten as

$$\frac{dx}{dt} = -\frac{\partial V(x,y,A)}{dx} + \sigma(x,y)\xi(t), \tag{11}$$

where $V(x,y,A)=\int \frac{f(z,y,A)}{\sigma^2(z,y)} dz$. The numerical calculation verifies that $V(x,y,A)$ is a double-well potential. Since y and A are nearly constant in contrast to the fast variable x, they can be regarded as two parameters in Eq. (10). For fixed y and A, there are points, $x_-(y,A)$, $x_+(y,A)$, and $x_0(y,A)$, satisfying $f(x,y,A)=0$. We assume $x_-(y,A)<x_0(y,A)<x_+(y,A)$. Note that the points $x_-(y,A)$ and $x_+(y,A)$ are always the local minima of the potential whereas $x_0(y,A)$ is the local maximum. Define

$$\Delta V_+ = V[x_0(y,A),y,A] - V[x_+(y,A),y,A],$$

$$\Delta V_- = V[x_0(y,A),y,A] - V[x_-(y,A),y,A].$$

Let B_L and B_R be the left-hand branch and right-hand branch of $f(x,y,A)=0$ in the phase plane (x,y), respectively. Due to the multiplicative or additive noise, jumps between the attraction basins of x_+ (right-hand well) and of x_- (left-hand well) by exceeding barriers will take place. In the case of multiplicative noise, if the trajectory is in the right-hand branch, then it subsequently slides along B_R until the fluctuation $\sigma(x,y)\xi(t)$ hopes the barrier ΔV_+ before it approaches to zero. With the increase of noise intensity, the probability of the fluctuation exceeding the barrier increases, leading to that the trajectory more early jumps to the left-hand branch B_L. However, $\sigma(x,y)\xi(t)$ is rather less noisy due to the comparatively small value of xy (especially in the case that the trajectory approaches to the point of $\Delta V_-=0$) when the trajectory is in the left-hand branch. Thereby, the hopping points from the left to the right almost keep invariant. In this case, the maximal activation protein x also almost keeps constant but the maximal activation protein y is sensitive to noise. In the case of additive noise, note that the additive noise does not depend on the system variable. The trajectory slides down the left-hand branch and the potential difference ΔV_- approaches to zero. With the increase of noise intensity, the trajectory shows the increasing probability of jumping to the right branch, leading to the decrease of the maximal activation protein x. In this case, since ΔV_+ and ΔV_- are not symmetrical, the system needs larger noise intensity to exceed the barrier from the right branch to the left branch. With this inherent property, the maximal activation protein y exhibits smaller variation in contrast to the activation protein x.

A. Effect of both noise and cell density on coherence and collective rhythm

Before showing how the coherence and cooperative dynamics of the interacting genetic oscillators depend on cell density and noise intensity, we need a few characteristic indices. To characterize the collective behaviors across a population, we first introduce the instantaneous phase of the dynamics for each cell [32]

$$\phi_i(t) = 2\pi \frac{t-\tau_k^i}{\tau_{k+1}^i - \tau_k^i} + 2\pi k, \quad \tau_k^i < t \leq \tau_{k+1}^i, \tag{12}$$

where τ_k^i is the time until the kth firing of the ith cell, which is defined in simulations as the moment of crossing the threshold of $x_i(t)=2.0$. Then, we define an order parameter to measure the phase synchronization of the coupled stochastic genetic oscillators [46],

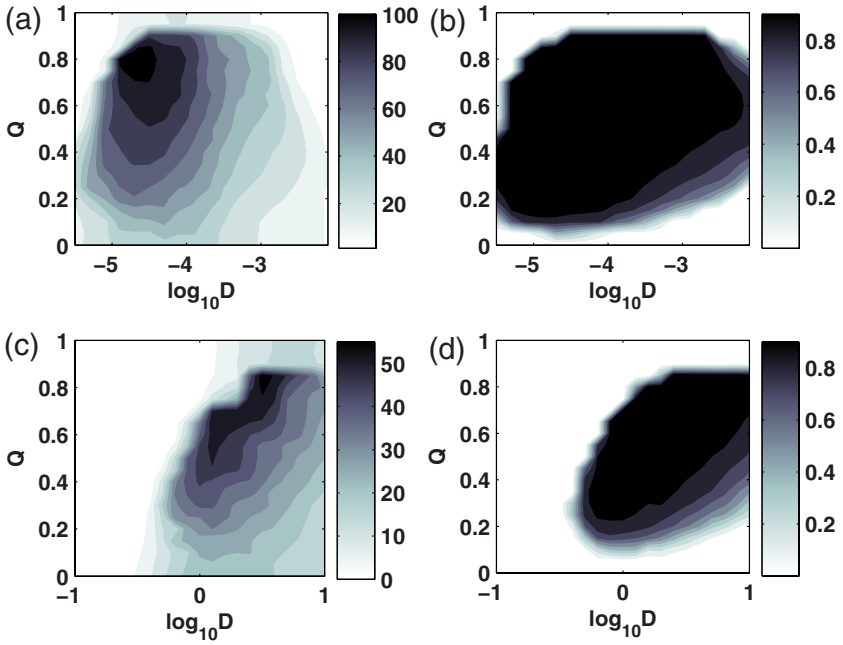

FIG. 6. (Color online) The dependence of signal-to-noise ratio S and order parameter R on noise intensity D and cell density Q: (a, c) S as a function of D and Q in the cases of multiplicative and additive noises, respectively; (b, d) R vs both D and Q for multiplicative and additive noises, respectively.

$$R = \left| \frac{1}{N} \sum_{k=1}^{N} e^{i\phi_k} \right|. \tag{13}$$

In this way, $R \approx 0$ in the unsynchronized regime whereas $R \approx 1$ in the synchronized case. In addition, we compute the coherence factor S of the population, based on the distribution of pulse intervals T_k^i for all N cells, i.e., $S = \overline{S^i}$, where S^i represents the signal-to-noise ratio of the ith cell as defined by Eq. (3), and the overbar stands for the ensemble average over cells.

The effects of the noise intensity D and the cell density Q on signal-to-noise S and order parameter R are summarized in Fig. 6, where different colored regions in the parameter space (D, Q) are shown for an ensemble of $N=100$ cells. Figures 6(a) and 6(c) show how S depends on D and Q, where the bar on the right-hand side indicates the different values of the signal-to-noise ratio with different colors in the cases of multiplicative and additive noises, respectively. Figures 6(b) and 6(d) show how R depends on D and Q, where the bar on the right-hand side indicates the different values of the order parameter with different colors. In the case of multiplicative noise, for most of the fixed cell densities Q, S increases first, then reaches a maximum, and then decreases with the increase of the noise intensity D, displaying a typical self-induced stochastic resonance effect. Similarly, for some of fixed noise intensities D, S first increases with the increase of the cell density Q until it reaches an optimal value. After that, it decreases gradually. On the other hand, the synchronization index R also has similar tendency in the parameter space (D, Q), as shown in Fig. 6(b). In contrast, in the case of additive noise, the S and R almost have the completely similar characteristics as described in the case of multiplicative noise, referring to Figs. 6(c) and 6(d). In addition, we point out that in the cases of these two kinds of noises, the noise-induced stochastic oscillation of individual units in a population can be explained essentially by the SISR mechanism. Due to the similar characteristics of S and R in both cases, below we focus on analyzing the dynamics induced by the multiplicative noise in details.

From Figs. 6(a) and 6(b), one can observe several dynamical regimes labeled by different colors. For clarity, we examine two different lines in Figs. 6(a) and 6(b): One horizonal line where the cell density Q is fixed but the noise intensity is variable, and one vertical line where the noise intensity D is fixed but the cell density is changeable.

First, we examine a particular horizonal line with $Q=0.7$. For a low noise intensity ($D < 10^{-5.2}$), the motion of the cells is essentially less coherent and independent because the stochastic behaviors governed by noise in the individual cells show a large variation. In this case, the cell-cell communication cannot bring out any collective behavior. Owing to such a nearly independent motion, the phase differences among cells have a uniform random distribution on $(0, 2\pi)$, resulting in $R \approx 0$ [see the bar in Fig. 6(b)]. A typical temporal pattern of x_i corresponding to this case is displayed in Fig. 7(a), which shows that the temporal pattern of each cell is rather irregular and independent of others because of a weak noise. For a moderate noise intensity, the entire system becomes sensitive to noise because the pulse that events arise from the fluctuation within one cell now become the source of exciting the other cells. As a consequence, this global excitation enhances the coherence and collective behaviors of the cells, as indicated by the simultaneous increase of S and R [referring the bars in Figs. 6(a) and 6(b)]. A pronounced SISR scenario and synchronization emerge, as shown in Fig. 7(b). In contrast to Figs. 2(a) and 5(a), the coherence in the ensemble of genetic oscillators via the cellular communication is better than that in the single stochastic oscillator for most of the parameter values. The gain of S is a consequence of communication-enhanced coherence, which is similar to the famous array-enhanced coherence resonance [47–50]. However, with the further increase of noise intensity, the coherence is ruined but the synchronization holds on, referring to Fig. 7(c).

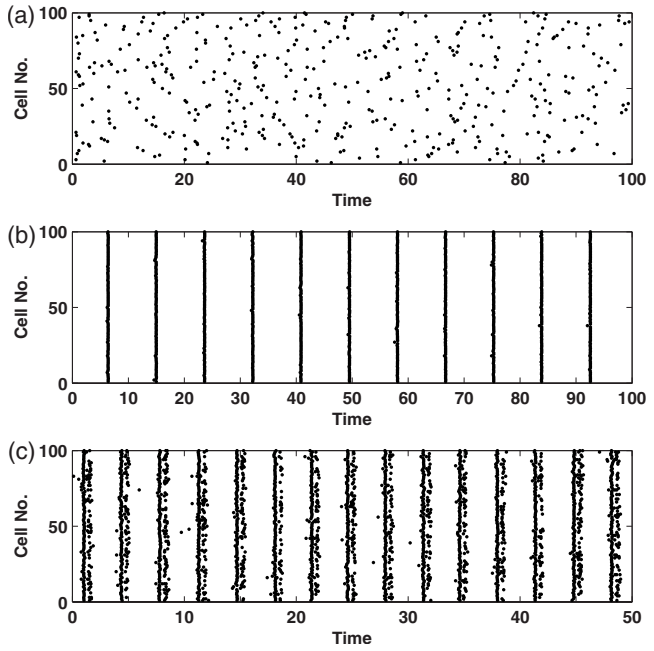

FIG. 7. Temporal firing patterns corresponding to Fig. 6. (a) $Q=0.7$, $D=10^{-5.3}$, (b) $Q=0.7$, $D=10^{-4.5}$, (c) $Q=0.7$, $D=10^{-2.0}$.

Then, we examine a particular vertical line with the noise intensity $D=10^{-4.0}$. Three typical temporal patterns for low, moderate, and high cell densities are shown in Figs. 8(a)–8(c), respectively. For a low cell density, the motion of the individual cells is essentially independent because a noise-induced pulse within a cell is insufficient to excite the ones of the other cells, as shown in Fig. 8(a). With a moderate cell density, the system displays better coherence and even perfect synchronization, as shown in Fig. 8(b), which is

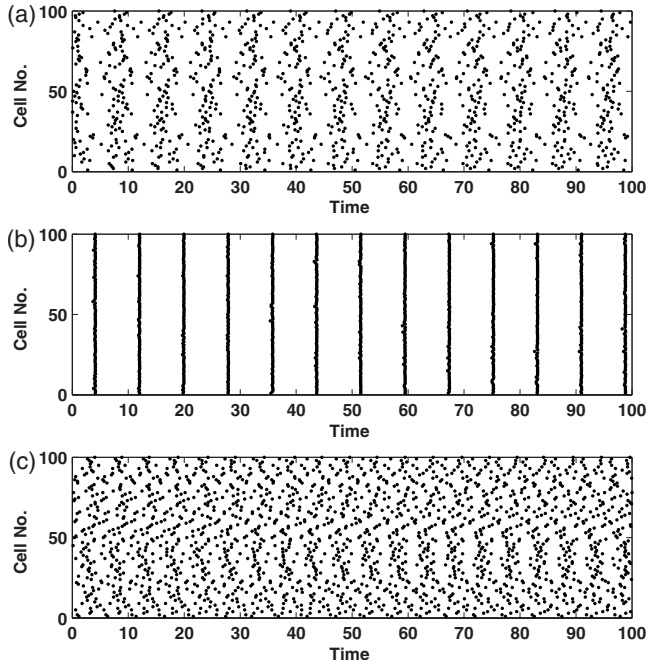

FIG. 8. Temporal firing patterns corresponding to Fig. 6. (a) $D=10^{-4.0}$, $Q=0.05$, (b) $D=10^{-4.0}$, $Q=0.50$, (c) $D=10^{-4.0}$, $Q=0.98$.

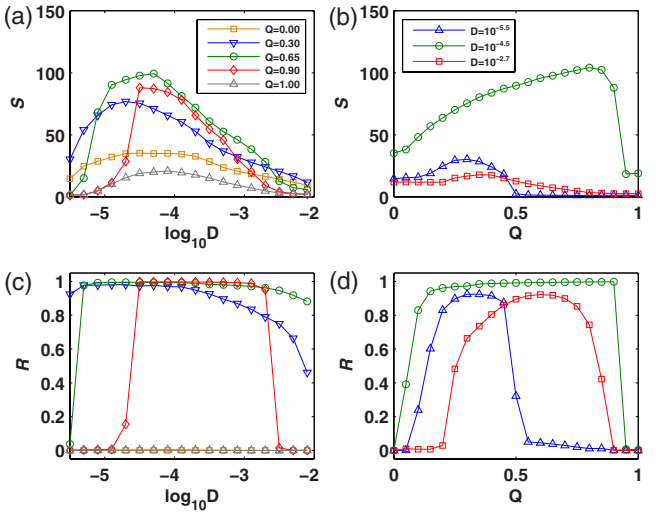

FIG. 9. (Color online) The dependence of signal-to-noise ratio S and order parameter R on noise intensity D for several cell densities and on cell density Q for several noise intensities: (a) S vs D; (b) S vs Q; (c) R vs D; (d) R vs Q. The legends in (a) and (b) are also applicable to (c) and (d), respectively.

similar to the pattern shown in Fig. 7(b). This is, in this case, because both D and Q fall into the parameter space (D,Q) with more coherence and better synchronization. More interestingly, when the cell density approaches to saturation, the coherence and synchronization suddenly disappear for arbitrary noise intensity, as shown in Fig. 8(c). This is counterintuitive since coupling is conventionally believed to favor collective behaviors.

B. Noise can serve as a controller for coherence and collective rhythm

To show how noise plays a controller role for collective rhythm and coherence across an ensemble of stochastic genetic oscillators, we also examine horizonal and vertical lines in Figs. 6(a) and 6(b).

Figures 9(a) and 9(c) show the dependence of the signal-to-noise ratio S and the order parameter S on the noise intensity D, respectively, for several different cell densities Q. We observe the following several characteristics: (1) Without cellular communication (i.e., $Q=0$) and if the cell density is very large (e.g., $Q\approx 1$), then the population of stochastic oscillators cannot achieve synchronization [see Fig. 9(c)] and the coherence of the entire system is very poor [refer to Fig. 9(a)]. The results in the $Q\approx 1$ case are also counterintuitive since the coupling is conventionally thought of as favoring collective behaviors. (2) For a fixed moderate cell density, there exists an optimal noise intensity such that the coherence index S has a maximum. (3) For a fixed moderate cell density, there exists a wide region of the noise intensity in which the synchronization index R is nearly equal to 1. In other words, in this region, the synchronization in the sense of statistics is achieved. (4) The synchronization region with respect to the noise intensity is not enlarged with the increase of the cell density.

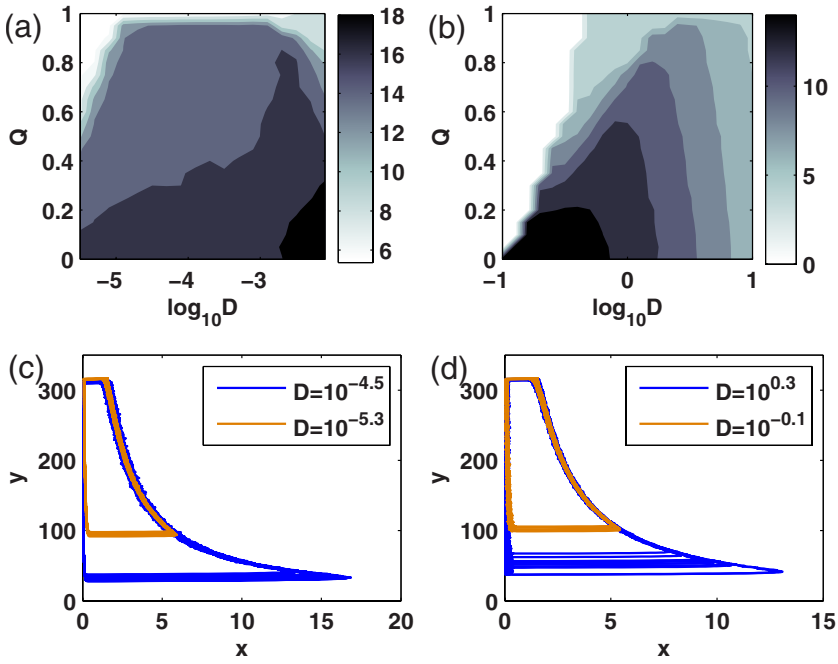

FIG. 10. (Color online) Noise-induced stochastic limit cycles with different amplitudes in the cases of multiplicative noise (a,c) and additive noise (b,d): (a,b) The dependence of the mean amplitude of the component x on the parameters D and Q in the cases of multiplicative and additive noises, respectively, where the right-hand bar indicates the values of the mean amplitude; (c,d) phase diagrams of two typically different noise-induced limit cycles by choosing two noise intensities in the cases of multiplicative and additive noises, respectively, where, $Q=0.8$ is fixed.

Figures 9(b) and 9(d) show the dependence of the signal-to-noise ratio S and the order parameter R on the cell density Q, respectively, for several different noise intensities D

Interestingly, in the case of a low or high cell density, the synchronization cannot be achieved even for arbitrary noise intensity. In particular, for a weak noise intensity, there exists a narrow region of cell density in which synchronization emerges [see the blue curve in Fig. 9(d)]. For a moderate noise intensity, there is a wider region of the cell density such that the synchronization index R nearly approaches to 1, but the region is narrowed as the noise intensity increases. On the other hand, for a weak or strong noise intensity, it seems that S has comparatively small maximum [see the blue and red curves in Fig. 9(b)]. For a moderate noise intensity, however, there exist a wider region of cell density such that S has a larger value. In other words, the cell density remarkably affects the coherence only for a moderate noise intensity. Such a role of the cell density seems different from that in the case of coupled stochastic FitzHugh-Nagumo oscillators where the coupling can enhance the coherence [47,48].

C. Noise-induced stochastic limit cycles with different amplitudes

From the previous analysis, we have seen that the cooperativity between noise and cell density not only can induce collective rhythms but also can enhance coherence. In this section, we show another constructive role of multiplicative or additive noise, i.e., different noise intensities can induce different kinds of stochastic limit cycles for a high cell density. More precisely, in the case of multiplicative noise [similarly in the case of additive noise, referring to Figs. 10(b) and 10(d)], there are several regions of the plane (D,Q) in which there exists noise-induced limit cycles with different amplitudes of the component x [refer to Fig. 10(a)]. For example, for the cell density $Q=0.8$ [i.e., a horizonal line in Figs. 10(a) and 10(b)], the amplitude of the component x of individual elements in the population shows a rapid transition from low to high with the increase of noise intensity, referring to Figs. 10(a) and 10(b). Figure 10(c) clearly shows that two different noise intensities $D=10^{-5.3}$ and $D=10^{-4.5}$ induce two different types of limit cycles: The one is with a large amplitude and the other is with a small amplitude. Note that in the case of low amplitude of the component x, the entire system shows unsynchronized oscillation due to the rather irregular oscillation of individual stochastic oscillators [see Figs. 6(b) and 6(d)]. The similar phenomena are also illustrated in Figs. 10(b) and 10(d). Such phenomena seem to be first found in a population of stochastic genetic oscillators coupled to the quorum-sensing mechanism, and meanwhile also would imply a biological fact that noise can autonomously adjust the intracellular process so as to adopt the cellular environment stress. Similarly, by examining one vertical line of Figs. 10(a) and 10(b), we see that the high cell density Q can serve as an effective parameter to damp the amplitude of stochastic oscillators. This possibly implies another biological fact that in the cellular environment with a high cell density, a mass of cells competing for the limited nutrition would lead to an abnormally low amplitude response.

IV. REPULSIVE COUPLING: CHARACTERISTICS OF PHASE DIFFERENCE DISTRIBUTION

First, to distinguish repulsive coupling from attractive coupling, we make some explanations. Coupling is attractive if any two of the coupled oscillators (including stochastic oscillators) prefer in-phase configuration, and otherwise repulsive. For example, attractive coupling can force coupled stochastic oscillators to reach a stochastic synchronization state as seen in the preceding sections. In contrast, repulsive coupling tends to enlarge the phase difference between interacting stochastic oscillators. Then, we point out that coupled

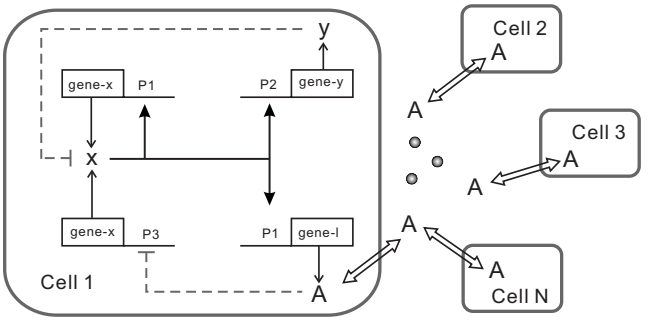

FIG. 11. Scheme for a population of stochastic genetic oscillators coupled to a quorum-sensing apparatus via repulsive phase.

oscillators with repulsive coupling can appear in many fields, such as physics [51], electronics [52], and chemistry [53]. Examples of repulsive coupling include multimode lasers [54] and saline oscillators [55]. Repulsive coupling can be also used to explain morphogenesis in hydra regeneration and animal coat pattern formation [56,57]. However, there are few works devoted to studying the dynamics of populations of stochastic genetic oscillators via phase-repulsive cellular communication.

In contrast to Ref. [25], here we propose a feasible synthetic genetic network via the cell-to-cell communication module that is designed to have a repressive and phase-repulsive effect. The corresponding gene regulatory network is shown in Fig. 11.

The mathematical equations corresponding to Fig. 11 are the same as Eqs. (4)–(7) but $\rho_1=0$ due to phase-repulsive communication between cells. As is done previously, we first introduce the instantaneous phase of dynamics for each cell [refer to Eq. (12)]. Then, we introduce a phase difference between arbitrarily two stochastic oscillators,

$$\Delta\phi_{ij}(t) = \phi_i(t) - \phi_j(t), \quad i,j = 1,2,\ldots,N. \tag{14}$$

For the convenience and clarity of description, we instead introduce a stochastic variable of phase difference in contrast to Ref. [58],

$$\Delta\phi(t) \in \{\Delta\phi_{i,i_0}(t) \bmod 2\pi, i \neq i_0\}, \tag{15}$$

where i_0 is an arbitrarily chosen index for which the corresponding stochastic oscillator is taken as a reference. We denote by $p(\Delta\phi)$ the corresponding distribution function or probability density that can show the effect of repulsive coupling. Then, $p(\Delta\phi)$ obeys a distribution over $[0,2\pi]$. In such a distribution displayed with a histogram, the preferred phase differences are manifested by peaks and the sharpness of the distribution characterizing the degree of the stochastic phase locking or clustering. We are interested in the effect of noise intensity on the characteristics of $p(\Delta\phi)$. We point out that the synchronization index as defined in Eq. (13) for describing collective behaviors of a population is inappropriate or even invalid in the case of repulsively coupled stochastic oscillators. In numerical simulations, the parameter values except for the cell density Q and the noise intensity D are the same as previously, and the initial conditions are arbitrarily chosen.

Furthermore, in order to characterize how pronounced the peaks are in the phase difference probability distribution, we introduce a useful index: Shannon entropy (sometimes referred to as a measure of uncertainty [59]). It is known that the Shannon entropy plays a central role in information theory. The entropy of a random variable is defined in terms of its probability distribution, and can show a good measure of randomness or uncertainty. We calculate the Shannon entropy with the probability distribution of the phase differences among stochastic oscillators [60]

$$E = -\sum_{k=1}^{N_b} p_k \log_2(p_k), \tag{16}$$

where N_b (=100 in our numerical simulation) is the number of bins used to determine the probability distribution, and p_k is the probability that the wrapped phase difference falls into the bin. It is noted that the maximal entropy ($E_{\max}$) corresponding to a uniform distribution [equal to $\log_2(100)$ or 6.6439 for $N_b=100$].

Regarding the effect of repulsive coupling on collective rhythms, it has been shown that the repulsive coupling can induce clustering across a population of deterministic limit-cycle oscillators. Here, for populations of stochastic oscillators we mainly analyze the characteristics of the phase difference distribution function $p(\Delta\phi)$ which describes the phase relationship between arbitrary stochastic oscillators in the sense of statistics, and present some interesting phenomena.

In the case of attractive coupling, we have studied a population of genetic stochastic oscillators induced by additive or multiplicative noise. It has been shown that attractive coupling can greatly enhance the noise-induced coherence. A naturally arising question is whether or not the coherence can be also enhanced by intracellular communication in the case of repulsive coupling? Due to the same mechanism of noise-induced oscillation and the similar qualitative natures for phase difference distribution in the cases of multiplicative and additive noises, below we investigate only the effect of multiplicative noise and pay less attention to the detailed difference between both noises. Throughout this section, we set $\alpha_1=10$, $\alpha_2=1$, $\alpha_3=50$, $\alpha_4=0.4$, $\beta_1=0.5$, $\beta_2=0.5$, $\beta_3=25$, $\beta_4=0.2$, $\rho=200$, $\rho_1=0$, $\gamma=3.0$, $\mu=10$, $n=4$, $\eta_{\text{int}}=120$. In addition, we point out that the following investigations of phase difference distribution in two particular cases of the cell number $N=2$ and 3 is only to better understand the phase-repulsive relationship between stochastic oscillators. In these two particular cases, the relation between the parameter Q and the cell density should be understood according to the following explanations: if Q changes, then the cell volume must accordingly change so that N is invariant, according to the previous definition of Q.

In order to characterize the effect of repulsive coupling on the coherence of the individual oscillators, we calculate S as a function of cell density Q and noise intensity D. Figures 12(a) and 12(b) show S vs Q and D for the system consisting of Eqs. (4)–(6) and Eq. (9) with $\rho_1=0$ and the population of 100 interacting oscillators, respectively. The SISR effect can be used to explain that S has a maximum in the interval of

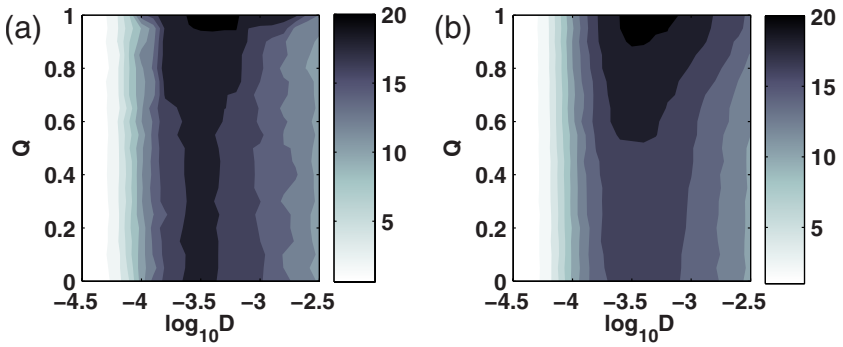

FIG. 12. (Color online) The dependence of signal-to-noise ratio S on noise intensity D and cell density Q for (a) the auxiliary system; (b) the coupled system with $N=100$.

the noise intensity D for a fixed cell density Q in both cases. Note that Q does not have the significant effect on S for a fixed D, referring to Figs. 12(a) and 12(b). In addition, compared with Fig. 12(a), Fig. 12(b) shows that the repulsive coupling has negligible effect on S. The results shown in Figs. 12(a) and 12(b), however, are significantly different from those in the case of attractive coupling.

A. Unimodal distribution of phase differences in the case of two oscillators

In the case of two stochastic oscillators, the main characteristic of collective behaviors is that the distribution of phase differences display stochastic antiphase in the sense of statistics. In other words, the phase difference between the two stochastic oscillators obeys the distribution concentrated at π over $[0,2\pi]$, or the firings between the two oscillators appear in the inverse correlation (i.e., the correlation coefficient between two time series is negative), which is similar to antiphase synchronization of two coupled neurons with channel noise [61]. Specifically, if one stochastic oscillator is firing at a time, then the other stochastic oscillator has no pulse at the time. To effectively show the effect of noise and cell density on the phase distribution, we calculate the Shannon entropy as a function of noise intensity and cell density, as plotted in Fig. 13(a). It is clearly observed that there is a region in the parameter space (D,Q) where the Shannon entropy is globally minimal. In other words, there exists an optimal region in which the two stochastic oscillators have optimal antiphase relationship. For example, for the fixed $Q=0.8$, the Shannon entropy shown in Fig. 13(b) has a minimum with respect to the noise intensity. In this case, three examples of phase distribution for three different noise intensities display the antiphase stochastic oscillation, as shown in Figs. 13(c)–13(e), respectively. Note that with the gradual increase of D, the shape of the distribution function $p(\Delta\phi)$ would be distorted, but $p(\Delta\phi)$ is still antiphase [see Fig. 13(e)]. We point out that the distorted peak would arise from the combined effect of self-induced stochastic resonance and repulsive coupling, where the mean period of stochastic oscillators is susceptible to noise through the SISR mechanism, and the different relative firing events, i.e., the different peaks of the distribution, are attributed to the effect of repulsive coupling. For Figs. 13(c)–13(e), the corresponding temporal firing patterns are plotted in Fig. 13(f).

B. Bimodal distribution of phase differences in the case of three oscillators

In this section, we consider three stochastic genetic oscillators with phase-repulsive cellular communication. Reference [62] has shown that three repulsively coupled deterministic oscillators can demonstrate different attractors. Also, Ref. [52] has displayed that several additional attractors can arise when three repulsively coupled relaxators are detuned. Accordingly, we can expect that three interacting stochastic genetic oscillators have richer dynamical behaviors due to the joint effect of phase-repulsive cellular communication and noise. In this case, the main feature of noise-induced coherent motions is that the phase difference distribution displays bimodality. For a weak noise intensity, e.g., $D=10^{-3.5}$, the phase difference distribution function $p(\Delta\phi)$ displays two peaks as seen in Fig. 14(a). With a small increase of the noise intensity, e.g., $D=10^{-3.0}$, two peaks become sharper, implying that the phase relationship among the three stochastic oscillators becomes more explicit, referring to Fig. 14(b). However, for the higher noise intensity, e.g., $D=10^{-2.5}$, the noise has a destructive effect on the phase relationship, i.e., the sharpness of the two peaks is blurred. More precisely, for the fixed cell density $Q=0.8$ the bimodality shown in Fig.

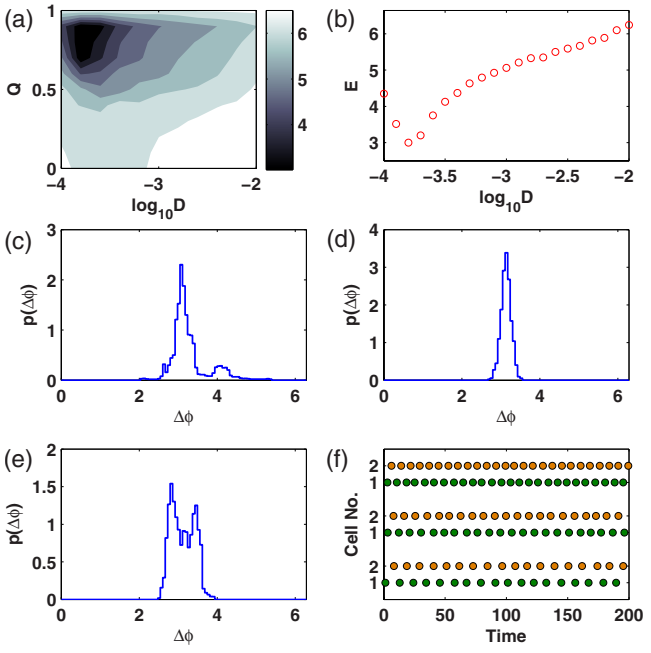

FIG. 13. (Color online) (a) The dependence of entropy E on noise intensity D and cell density Q; (b) E vs D for $Q=0.8$; (c) the phase difference distribution $p(\Delta\phi)$ as a function of $\Delta\phi$ for $Q=0.8$, $D=10^{-4.0}$; (d) $p(\Delta\phi)$ as a function of $\Delta\phi$ for $Q=0.8$, $D=10^{-3.8}$; (e) $p(\Delta\phi)$ as a function of $\Delta\phi$ for $Q=0.8$, $D=10^{-3.0}$; (f) raster plots for the cases (c, d, e) from bottom to top, respectively.

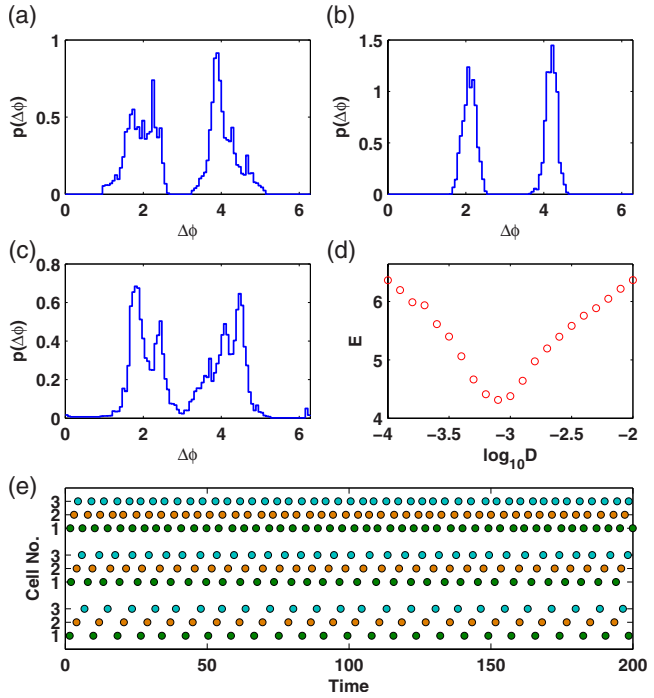

FIG. 14. (Color online) (a) The phase difference distribution $p(\Delta\phi)$ as a function of $\Delta\phi$ for $Q=0.8$, $D=10^{-3.5}$; (b) $p(\Delta\phi)$ as a function of $\Delta\phi$ for $Q=0.8$, $D=10^{-3.0}$; (c) $p(\Delta\phi)$ as a function of $\Delta\phi$ for $Q=0.8$, $D=10^{-2.5}$; (d) the dependence of Shannon entropy E vs noise intensity D for $Q=0.8$; (f) raster plots for case (a, b, c) from bottom to top, respectively.

14(b) is optimal whereas the bimodality displayed in Figs. 14(a) and 14(c) is distorted due to the effect of noise. To better illustrate the effect of noise on the phase distribution, we calculate the Shannon entropy E again, and plot the dependence between E and D for the fixed $Q=0.8$ in Fig. 14(d). Clearly, E has a minimum for a certain D. This further verifies that an optimal noise intensity induces the most regular phase relationship among the three repulsively coupled stochastic oscillators, analogous to that in the case of noise-induced coherent resonance.

In addition, we point out that there is a significant difference between two peaks observed both in the case of two stochastic oscillators [see Fig. 13(e)] and in the case of three stochastic oscillators (see Fig. 14). The former is due to the effect of strong noise whereas the latter results from the intrinsic nature of the phase difference distribution among the stochastic oscillators.

C. Polymodal distribution of phase difference in the case of multiple oscillators

In this section we numerically investigate the phase difference distribution in the case of multiple stochastic genetic oscillators with repulsive coupling via the quorum-sensing mechanism. In our numerical simulation, we simulate up to 100 stochastic oscillators, but the qualitative characteristics of the phase difference distribution function $p(\Delta\phi)$ are basically similar, when the cell number is beyond a threshold (the numerical simulation indicates that the threshold is 4). For clarity, here we only give the numerical results for the 10 stochastic oscillators with two kinds of noise intensities, as shown in Figs. 15(a) and 15(b), respectively.

For weak noise intensities, e.g., $D=10^{-4.0}$, the distribution function $p(\Delta\phi)$ is almost a flat curve with respect to the phase difference $\Delta\phi$, where there is no obvious peak (data are not shown). With the increase of noise intensity, e.g., $D=10^{-3.0}$, two peaks appear, referring to Fig. 15(a). For a larger noise intensity, three peaks appear, see Fig. 15(b). Note that two peaks in Fig. 15(a) imply that there exist two most probabilities of phase difference, whereas three peaks shown in Fig. 15(b) correspond to three most probabilities of phase difference. We point out that the appearance of two and three peaks in the phase difference distribution with appropriate noise intensities is the common feature for repulsively coupled multiple cells. Besides, we calculate the Sh-

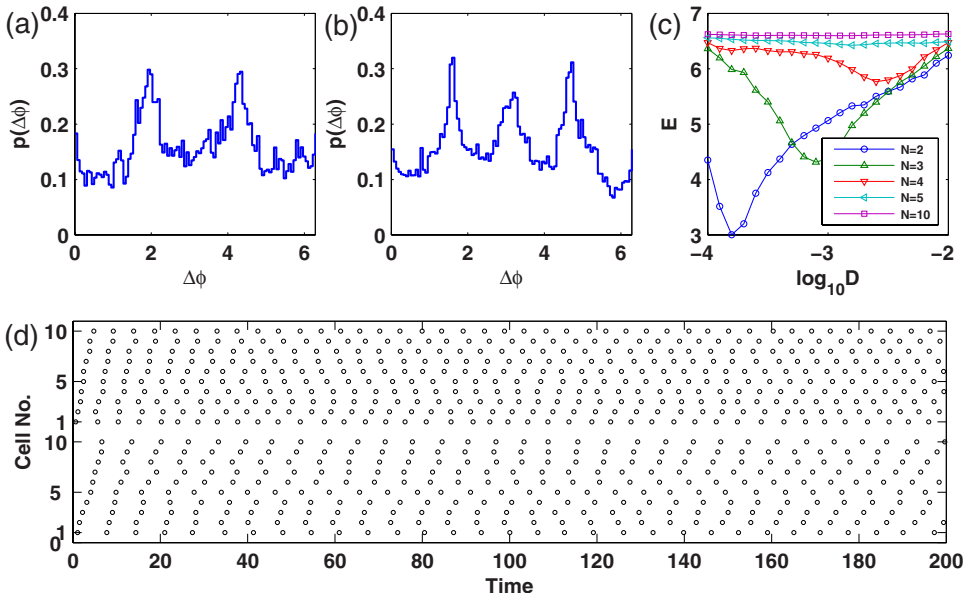

FIG. 15. (Color online) (a) The phase difference distribution $p(\Delta\phi)$ as a function of $\Delta\phi$ for $Q=0.8$, $D=10^{-3.0}$; (b) $p(\Delta\phi)$ as a function of $\Delta\phi$ for $Q=0.8$, $D=10^{-2.5}$; (c) The dependence of the Shannon entropy E on noise intensity D for several N with the fixed $Q=0.8$; (d) raster plots in the cases of (a, b) from bottom to top, respectively. For (a), (b), and (d), the cell number is $N=10$.

annon entropy again. Figure 15(c) shows the dependence of the Shannon entropy on noise intensity for some numbers of cells, i.e., $N=2,3,4,5,10$, where $Q=0.8$ is fixed. In the cases of $N=2$ and 3, the Shannon entropy has an apparent minimum but the minimum is not apparent for the larger cell number unless the related curves are locally zoomed. Actually, the minimum of the Shannon entropy with respect to D can approximate to the maximal Shannon entropy ($E_{\max}$) when the cell number is large enough, referring to Fig. 15(c). For the fixed cell number $N \geqslant 4$, both two and three peaks will appear in the phase difference distribution if we employ some noise intensities near the value of noise intensity corresponding to the minimal entropy. The corresponding temporal firing patterns of the component x of 10 stochastic oscillators with noise intensity $D=10^{-3.0}$ and $10^{-2.5}$ (from bottom to top) are shown in Fig. 15(d). The mechanism giving rise to the polymodal distribution may provide the statistical reliable relationship between phase differences for a cell population, but we can expect an intermittent transition between peaks of phase difference distribution of two oscillators, which in turn would provide a mechanism for cells to resist the environmental stress. Further study is needed to give a theoretical explanation of the observed phenomena in the case of the phase-repulsive coupling via quorum-sensing mechanism.

V. CONCLUSIONS AND DISCUSSIONS

We have shown that phase-attractive and phase-repulsive cell-to-cell communication have different effects on coherence and collective behaviors of an ensemble of stochastic relaxation-type genetic oscillators. In the case of attractive coupling, cellular communication can enhance both self-induced stochastic resonance and achieve robust collective rhythms. In particular, for fixed high cell densities, different intensities of noise resulting from the fluctuation of intrinsic chemical reactions or the extrinsic environment can induce stochastic limit cycles with different amplitudes in the sense statistics. In the case of repulsive coupling, the distribution function of phase difference among stochastic oscillators can display unimodality, bimodality or polymodality, depending on the noise intensity and the cell number.

For the core stochastic genetic oscillator used in our designing multicellular system, since noise is added to the equation of the fast variable, the noise-induced oscillation can be explained by the SISR mechanism recently found in the excitable FitzHugh-Nagumo system [17–19]. Therefore, it would be not surprising that some of the collective behaviors across populations of these stochastic oscillators via phase-attractive cellular communication are similar to those of interacting stochastic oscillators, referring to our recently finished work [63]. However, some communication-induced or noise-induced phenomena have been presented here.

In general, in the case of phase-repulsive coupling, the deterministic dynamics nature of population behaviors sensitively depends on the cell density. For example, Ref. [28] shows that different cell densities can induce oscillation, inhomogeneous limit cycles, clustering and single fixed point, respectively. In our cases, however, the distribution function of phase difference among stochastic oscillators with the different cell number can display different modalities, but there is a threshold of the cell number such that modality of the phase difference distribution basically keeps invariant as the cell number is beyond the threshold.

Finally, we point out that it would be worth investigating the joint effects of both internal and external noises and coupling on coherence and collective rhythms across populations of stochastic genetic oscillators.

ACKNOWLEDGMENT

This work was supported by the Natural Science Key Foundation of People's Republic of China (Contract No. 60736028).

[1] R. Milo, S. Shen-Orr, S. Itzkovitz, N. Kashtan, D. Chklovskii, and U. Alon, Science **298**, 824 (2002).
[2] R. Milo, S. Itzkovitz, N. Kashtan, R. Levitt, S. Shen-Orr, I. Ayzenshtat, M. Sheffer, and U. Alon, Science **303**, 1538 (2004).
[3] N. Maheshri and E. K. O'Shea, Annu. Rev. Biophys. Biomol. Struct. **36**, 413 (2007).
[4] J. R. Chabot, J. M. Pedraza, P. Luitel, and A. van Oudenaarden, Nature (London) **450**, 1249 (2007).
[5] A. Goldbeter, Nature (London) **420**, 238 (2002).
[6] M. B. Elowitz and S. Leibler, Nature (London) **403**, 335 (2000).
[7] M. R. Atkinson, M. A. Savageau, J. T. Myers, and A. J. Ninfa, Cell **113**, 597 (2003).
[8] E. Fung, W. W. Wong, J. K. Suen, T. Bulter, Sun-gu Lee, and J. C. Liao, Nature (London) **435**, 118 (2005).
[9] D. Bell-Pedersen, V. M. Cassone, D. J. Earnest, S. S. Golden, P. E. Hardin, T. L. Thomas, and M. J. Zoran, Nat. Rev. Genet. **6**, 544 (2005).
[10] J. R. Pomerening, S. Y. Kim, and J. E. Ferrell, Cell **122**, 565 (2005).
[11] J. Keener and J. Sneyd, *Mathematical Physiology* (Springer-Verlag, New York, 1998).
[12] L. Gammaitoni, P. Hänggi, P. Jung, and F. Marchesoni, Rev. Mod. Phys. **70**, 223 (1998).
[13] B. Lindner, J. García-Ojalvo, A. Neiman, and L. Schimansky-Geier, Phys. Rep. **392**, 321 (2004).
[14] F. Sagués, J. M. Sancho, and J. García-Ojalvo, Rev. Mod. Phys. **79**, 829 (2007).
[15] Hu Gang, T. Ditzinger, C. Z. Ning, and H. Haken, Phys. Rev. Lett. **71**, 807 (1993).
[16] A. S. Pikovsky and J. Kurths, Phys. Rev. Lett. **78**, 775 (1997).
[17] C. B. Muratov, E. V. Eijnden, and W. E, Physica D **210**, 227 (2005).
[18] R. E. Lee DeVille, E. Van den-Eijnden, and C. B. Muratov, Phys. Rev. E **72**, 031105 (2005).

[19] C. B. Muratov, E. V. Eijnden, and W. E, Proc. Natl. Acad. Sci. U.S.A. **104**, 702 (2007).
[20] G. M. Süel, J. García-Ojalvo, L. M. Liberman, and M. B. Elowitz, Nature (London) **440**, 545 (2007).
[21] H. Maamar, A. Raj, and D. Dubnau, Science **317**, 526 (2007).
[22] D. Schultz, E. Ben Jacob, J. N. Onuchic, and P. G. Wolynes, Proc. Natl. Acad. Sci. U.S.A. **104**, 17582 (2007).
[23] J. M. Vilar, H. Y. Kueh, N. Barkai, and S. Leibler, Proc. Natl. Acad. Sci. U.S.A. **99**, 5988 (2002).
[24] M. Scott, T. Hwa, and B. Ingalls, Proc. Natl. Acad. Sci. U.S.A. **104**, 7402 (2007).
[25] D. McMillen, N. Kopell, J. Hasty, and J. J. Collins, Proc. Natl. Acad. Sci. U.S.A. **99**, 679 (2002).
[26] J. García-Ojalvo, M. B. Elowitz, and S. H. Strogatz, Proc. Natl. Acad. Sci. U.S.A. **101**, 10955 (2004).
[27] T. S. Zhou, L. N. Chen, and K. Aihara, Phys. Rev. Lett. **95**, 178103 (2005).
[28] E. Ullner, A. Zaikin, E. I. Volkov, and J. García-Ojalvo, Phys. Rev. Lett. **99**, 148103 (2007).
[29] I. Leyva, I. Sendina-Nadal, J. A. Almendral, and M. A. F. Sanjuán, Phys. Rev. E **74**, 056112 (2006).
[30] P.-J. Kim, T.-W. Ko, H. Jeong, and H.-T. Moon, Phys. Rev. E **70**, 065201(R) (2004).
[31] A. T. Winfree, *The Geometry of Biological Time* (Springer, Berlin, 1980).
[32] A. S. Pikovsky, M. Rosenblum, and J. Kurths, *Synchronization—A Unified Approach to Nonlinear Science* (Cambridge University Press, Cambridge, 2001).
[33] J. Hasty, F. Isaacs, M. Dolnik, D. McMillen, and J. J. Collins, Chaos **11**, 207 (2001).
[34] J. Hasty, J. Pradines, M. Dolnik, and J. J. Collins, Proc. Natl. Acad. Sci. U.S.A. **97**, 2075 (2000).
[35] M. Kaern, T. C. Elston, W. J. Blake, and J. J. Collins, Nat. Rev. Genet. **6**, 451 (2005).
[36] J. M. Raser and E. K. O'Shea, Science **309**, 2010 (2005).
[37] C. W. Gardiner, *Handbook of Stochastic Methods for Physics, Chemistry and the Natural Sciences*, 3rd ed. (Springer-Verlag, Berlin 1985).
[38] N. G. van Kampen, *Stochastic Processes in Physics and Chemistry* (North-Holland, Amsterdam, 1981).
[39] P. E. Kloeden and E. Platen, *Numerical Solution of Stochastic Differential Equations* (Springer-Verlag, Berlin, 1992).
[40] A. Kuznetsov, M. Kaern, and N. Kopell, SIAM J. Appl. Math. **65**, 392 (2004).
[41] T. S. Zhou, J. J. Zhang, Z. J. Yuan, and A. L. Xu, PLoS ONE **2**, e231 (2007).
[42] J. Rinzel and G. B. Ermentrout, in *Analysis of Neural Excitability and Oscillations, Methods in Neuronal Modeling*, edited by C. Koch and I. Segev (MIT, Cambridge, MA, 1989).
[43] E. M. Izhikevich, Int. J. Bifurcation Chaos Appl. Sci. Eng. **10**, 1171 (2000).
[44] R. Guantes and J. F. Poyatos, PLOS Comput. Biol. **2**, 3:e30 (2006).
[45] M. I. Freidlin, J. Stat. Phys. **103**, 283 (2000).
[46] Y. Kuramoto, *Chemical Oscillations, Waves and Turbulence* (Springer-Verlag, Berlin, 1984).
[47] B. Hu and C. S. Zhou, Phys. Rev. E **61**, R1001 (2000).
[48] C. S. Zhou, J. Kurths, and B. Hu, Phys. Rev. Lett. **87**, 098101 (2001).
[49] Y. Shinohara, T. Kanamaru, H. Suzuki, T. Horita, and K. Aihara, Phys. Rev. E **65**, 051906 (2002).
[50] O. Kwon, H.-H. Jo, and H.-T. Moon, Phys. Rev. E **72**, 066121 (2005).
[51] B. S. Kerner and V. V. Osipov, Usp. Fiz. Nauk **160**, 1 (1990).
[52] D. Ruwisch, M. Bode, D. Volkov, and E. Volkov, Int. J. Bifurcation Chaos Appl. Sci. Eng. **9**, 1969 (1999).
[53] V. K. Vanag, L. F. Yang, M. Dolnik, A. M. Zhabotinsky, and I. R. Epstein, Nature (London) **406**, 389 (2000).
[54] K. Wiesenfeld, C. Bracikowski, G. James, and R. Roy, Phys. Rev. Lett. **65**, 1749 (1990).
[55] K. Yoshikawa, N. Oyama, M. Shoji, and S. Nakata, Am. J. Phys. **59**, 137 (1991).
[56] H. Meinhardt, *Models of Biological Pattern Formation* (Academic Press, London, 1982).
[57] A. J. Koch and H. Meinhardt, Rev. Mod. Phys. **66**, 1481 (1994).
[58] C. S. Zhou and J. Kurths, Phys. Rev. E **65**, 040101(R) (2002).
[59] C. E. Shannon, Bell Syst. Tech. J. **27**, 379 (1948); **27**, 623 (1948).
[60] G. Balazsi, A. Cornell-Bell, A. B. Neiman, and F. Moss, Phys. Rev. E **64**, 041912 (2001).
[61] L. C. Yu, Y. Chen, and P. Zhang, Eur. Phys. J. B **59**, 249 (2007).
[62] E. I. Volkov and M. N. Stolyarov, Phys. Lett. A **159**, 61 (1991).
[63] J. J. Zhang, Z. J. Yuan, J. W. Wang, and T. S. Zhou, Phys. Rev. E **77**, 021101 (2008).